Research Square

Preprints are preliminary reports that have not undergone peer review.
They should not be considered conclusive, used to inform clinical practice,
or referenced by the media as validated information.

Waste wheat fermentation starter valorization: Conversion into regenerable biochar for CO_2 capture

Dexin Xu
China University of Mining and Technology
Xuyao Qi
qixuyao@cumt.edu.cn
China University of Mining and Technology
Mujun Chen
China University of Mining and Technology
Chunxi Wu
China University of Mining and Technology
Lanjun Zhang
Jiangsu Ocean University
Fusheng Wang
North China University of Science and Technology
Leilin Zhang
Anhui University of Science and Technology
Yaqi Qin
China University of Mining and Technology

Research Article

Keywords: Jiuqu waste, Biochar, CO2 adsorption, Response surface optimization

Posted Date: November 27th, 2026

DOI: https://doi.org/10.21203/rs.3.rs-11792268/v1

License: This work is licensed under a Creative Commons Attribution 4.0 International License.
Read Full License

Additional Declarations: No competing interests reported.

Abstract

Converting waste wheat fermentation starter into reusable adsorbents provides an opportunity to recover material value from fermentation waste while developing sorbents for CO_2 capture. Here, waste wheat fermentation starter was valorized into biochar (Bio@JQ) through direct pyrolysis under nitrogen without externally added activating or doping agents. A three-factor Box–Behnken design was employed to optimize the BET specific surface area by varying pyrolysis temperature, nitrogen flow rate, and heating rate. The selected biochar exhibited a BET specific surface area of 141.93 $m^2\ g^{-1}$ and a total pore volume of 0.0568 $cm^3\ g^{-1}$. Structural characterization revealed a disordered carbon framework with accessible micropores and retained nitrogen- and oxygen-containing surface species. At 1 bar, Bio@JQ achieved CO_2 adsorption capacities of 2.32, 1.76, and 1.36 mmol g^{-1} at 273.15, 303.15, and 318.15 K, respectively, with the temperature-dependent uptake indicating exothermic adsorption. The combined structural and adsorption results were consistent with micropore filling and noncovalent interactions, with surface heteroatoms potentially contributing to CO_2 affinity. Bio@JQ retained 91.88% of its initial adsorption capacity after 45 adsorption–regeneration cycles, demonstrating repeated use under the tested conditions. These findings demonstrate the feasibility of converting waste wheat fermentation starter into a regenerable CO_2 adsorbent through an activation-free pyrolysis route, linking fermentation-waste valorization with the development of reusable carbon-based sorbents.

1. Introduction

Carbon dioxide (CO_2) emissions from fossil fuel use are a major driver of global climate change. Reducing carbon emissions from fossil fuel use and associated industrial processes remains an important task during the transition toward cleaner energy systems [1]. Carbon capture, utilization, and storage (CCUS) provides an important technological pathway for reducing CO_2 emissions from stationary sources. Among available technologies, adsorption has attracted considerable attention for post-combustion CO_2 capture because of its operational flexibility, adsorbent regenerability, and potential for reducing separation energy requirements. Adsorbent pore structure, surface chemistry, and regeneration performance directly affect capture efficiency [2, 3]. Developing solid adsorbents that balance adsorption performance, cycling stability, and production costs is therefore essential for advancing the practical application of adsorption-based CO_2 capture.

Solid adsorbents used for CO_2 capture primarily include metal–organic frameworks, zeolites, metal oxides, porous polymers, and carbon materials [4]. Biochar can be produced from biomass waste, and its pore structure and surface chemistry can be tailored through preparation conditions, providing a pathway that integrates waste valorization with CO_2 capture. However, the adsorption performance of some biochars produced by direct pyrolysis is constrained by feedstock composition and pyrolysis conditions. Insufficient accessible microporosity, unsuitable pore size distributions, and limited effective surface sites can restrict their CO_2 adsorption capacity at low partial pressures. For porous carbon materials, CO_2 adsorption depends on specific surface area, the distribution of narrow micropores and

ultramicropores, pore accessibility, and the types of surface functional groups [5, 6]. Coordinated control of pore structure and surface chemistry is therefore an important approach to improving CO_2 adsorption by biochar. Numerous studies have demonstrated that microwave pyrolysis, steam activation, ball milling, ultrasonication, and chemical activation can improve biochar specific surface area, pore structure, and surface chemistry, thereby enhancing CO_2 adsorption performance [7–9]. Luo, Fierro, Jonnalagadda, and colleagues reported that alkaline earth metals, such as Mg and Ca, can increase the abundance of basic surface sites and enhance adsorption affinity for CO_2 [10–12]. Ahmed, Li, Zhang, and colleagues found that transition metals, such as Ni and Fe, can further regulate interfacial electronic structure and surface polarity, strengthening interactions between the material and CO_2 [13–15]. Introducing active metal sites through impregnation, hydrothermal processing, biomineralization, or in situ growth can improve pore structure and promote the reorganization of surface functional groups, thereby enhancing CO_2 adsorption capacity and cycling stability.

However, these performance gains often entail additional processing requirements. For example, alkali activation may increase chemical consumption and require equipment with greater corrosion resistance, while subsequent washing requires water and treatment of saline wastewater [16]. Metal loading requires careful control of loading levels and dispersion to prevent particle aggregation or pore occupation from reducing the space available for adsorption [17]. Overall, prevailing modification strategies substantially increase total adsorbent production costs and extend processing workflows. They also introduce substantial secondary environmental burdens across the life cycle, fundamentally conflicting with the original goals of biomass waste valorization and low-carbon, environmentally responsible material development [18]. Reducing the use of externally added chemicals and simplifying preparation procedures while improving adsorption performance is therefore a direction that warrants attention in biochar adsorbent development [19]. Waste jiuqu offers a potential feedstock for exploring this preparation route. Produced through microbial fermentation of wheat and other grains, jiuqu contains carbohydrates, proteins, and other organic components that provide the precursors for carbon framework formation and the development of nitrogen- and oxygen-containing surface structures [20, 21]. Converting waste jiuqu into CO_2 adsorbents could expand its valorization pathways. However, precursor composition and morphology alone do not determine the adsorption performance of the resulting biochar. Its pore structure and surface sites also depend on component decomposition, volatile release, and carbon framework rearrangement during pyrolysis. In particular, pore development and functional group retention may respond differently to pyrolysis conditions [22]. Coordinating these responses is a key challenge in improving the adsorption performance of jiuqu-derived biochar through pyrolysis control. Pyrolysis temperature, heating rate, and protective gas flow rate jointly influence biomass thermal conversion. Pyrolysis temperature affects the extent of component decomposition and carbon structure evolution, whereas heating rate alters the course of thermal decomposition. Protective gas flow rate influences the removal of volatile products and their contact with the solid phase. Examining individual parameters alone cannot fully resolve their interactions or their combined effects on the properties of the final material. For jiuqu-derived biochar prepared without externally added chemicals, further research is needed to clarify how multiple processing parameters affect pore size

distribution and surface functional group composition, and how these structural changes jointly influence CO_2 adsorption [23]. Integrating process optimization, structural characterization, and adsorption mechanism analysis is therefore necessary to establish relationships among pyrolysis conditions, material structure, and adsorption performance.

Accordingly, this study proposes a new, green, one-step strategy for preparing high-performance porous biochar from jiuqu waste entirely through physical control of thermal processing conditions. Response surface methodology (RSM) was used to examine the individual and interactive effects of pyrolysis temperature, heating rate, and protective gas flow rate. Relationships between process parameters and CO_2 adsorption capacity were established, and optimal preparation conditions were identified within the experimental range. Pore structure analysis and SEM, XRD, XPS, and FTIR characterization were then used to investigate the microscopic morphology, carbon framework characteristics, and surface functional group composition of the optimized sample. Adsorption isotherms at different temperatures, isosteric heats of adsorption, and cyclic regeneration experiments were used to evaluate CO_2 adsorption performance and stability and to discuss the contributions of micropore filling and surface interactions. By integrating pyrolysis optimization with adsorption behavior analysis, this study aims to provide an experimental basis for valorizing waste jiuqu into CO_2 adsorbents.

2. Experimental methods and characterization

2.1 Materials and preparation

Jiuqu was collected from Guizhou Province, China, dried, ground, and sieved to obtain a 60–100 mesh fraction. A one-step high-temperature pyrolysis and activation method was used to convert jiuqu waste into functional biochar. Briefly, 10.0 g of the pretreated, dried jiuqu was placed in the reaction zone of a horizontal tube furnace. Pyrolytic carbonization and in situ thermal activation were conducted under a constant flow of high-purity N_2 at 200–500 mL min^{-1}. To systematically investigate the effects of pyrolysis thermodynamic and kinetic parameters on carbon microstructure evolution, a multifactor response surface methodology (RSM) experiment was designed using Design-Expert software. The heating rate was strictly controlled within a range of 5–9°C, and the pyrolysis activation temperature was set at 500–900°C. Samples were held at the target temperature for 100 min to promote carbon framework rearrangement, devolatilization, and extensive pore development. After the reaction, the samples were allowed to cool naturally to room temperature under the protective atmosphere. Standardized collection and drying procedures yielded a series of biochars modified by high-temperature pyrolysis, with progressively varying microscopic morphologies and controllable surface chemistry. The biochar prepared under the optimal processing conditions was designated Bio@JQ and used for subsequent physicochemical characterization, adsorption performance evaluation, and cycling durability tests.

2.2 Experimental design

A three-factor, three-level Box–Behnken response surface design was used to investigate and optimize the effects of preparation parameters on the BET specific surface area of biochar. Experimental design and statistical analysis were performed using Design-Expert software. Based on preliminary single-factor experiments, pyrolysis temperature, N_2 flow rate, and heating rate were selected as independent variables and designated X_1, X_2, and X_3, respectively. Each variable was evaluated at three coded levels: −1, 0, and + 1. The corresponding ranges were 500–900°C, 200–500 mL min^{-1}, and 5–9°C min^{-1}, respectively, with BET specific surface area (S_{BET}) as the response variable.

The Box–Behnken design comprised 15 runs, including 12 factor combinations and three replicate runs at the center point. The center-point replicates were used to estimate pure error and assess experimental repeatability. The detailed experimental design is presented in Table 1.

Table 1
Response surface experimental design

Experiment Number	Temperature (℃)	Flow rate (mL·min^{-1})	Heating rate (℃·min^{-1})
1	500	350	5
2	700	200	9
3	900	350	5
4	700	350	7
5	700	350	7
6	700	350	7
7	900	350	9
8	900	200	7
9	900	500	7
10	500	350	9
11	500	200	7
12	700	500	9
13	700	200	5
14	500	500	7
15	700	500	5

Analysis of variance (ANOVA) was used to assess the statistical significance of the model and individual regression terms, with $p < 0.05$ indicating statistical significance. Model fit and predictive performance were evaluated using the coefficient of determination (R^2), adjusted R^2 (R^2_{adj}), predicted R^2 (R^2_{pred}), and

the lack-of-fit test. Finally, numerical optimization was performed to identify the optimal factor settings for maximizing specific surface area, and validation experiments were conducted to assess model reliability.

2.3 Characterization

The pore structure of the samples was characterized using N_2 adsorption–desorption isotherms measured at 77 K with an automated surface area and pore size analyzer (BSD-660MG, Beishide Instrument Technology Co., Ltd., China). The specific surface area was calculated using the Brunauer–Emmett–Teller (BET) method, and additional parameters, including micropore volume and pore size distribution, were obtained. Surface morphology and microstructure were examined using scanning electron microscopy (ZEISS Sigma 500, Germany). Surface elemental composition and distribution were analyzed using the accompanying energy-dispersive X-ray spectrometer (Bruker D8 ADVANCE, Germany). Surface functional groups were identified using Fourier transform infrared spectroscopy (VERTEX 80V, Bruker, Germany). The degree of structural order and defect characteristics of the carbon materials were examined using Raman spectroscopy (DXR2xi, Thermo, USA). The surface chemical composition and changes in the chemical states of C, O, and Fe were analyzed using X-ray photoelectron spectroscopy (ESCALAB 250Xi, Thermo, USA).

2.4 CO_2 adsorption performance and calculation of isosteric heat of adsorption

CO_2 adsorption isotherms were measured at different temperatures using a BSD gas adsorption analyzer. Before measurement, the samples were degassed under vacuum at 150°C for 12 h to remove moisture and impurities adsorbed within the pores and on the surface. CO_2 uptake was then measured as a function of pressure at 0, 25, and 45°C, and adsorption performance was evaluated from the resulting isotherms.

The isosteric heat of CO_2 adsorption (Q_{st}) was calculated from the adsorption isotherms at different temperatures using the Clausius–Clapeyron equation [24, 25]:

$$Q_{st} = -R\left[\frac{\partial\, lnP}{\partial\left(\frac{1}{T}\right)}\right]_q$$

where Q_{st} is the isosteric heat of adsorption (kJ mol^{-1}), R is the ideal gas constant (8.314 J mol^{-1} K^{-1}), P is the equilibrium pressure at a specified uptake, T is the adsorption temperature, and q is the equilibrium CO_2 uptake.

3. Results and discussion

3.1 Rational design of biochar via pyrolysis regulation

The response surface analysis showed that the BET specific surface area of jiuqu-derived biochar depended on pyrolysis temperature, gas flow rate, and heating rate, together with their interactions. Pyrolysis temperature exerted the strongest influence, as shown in Fig. 2a and b. The BET specific surface area increased substantially as the temperature rose from 500 to approximately 650°C and remained high over 650–800°C. This trend may be associated with enhanced devolatilization and restructuring of the carbon framework, which promoted pore formation. Above 800°C, the specific surface area declined, potentially reflecting framework contraction and the collapse or coalescence of existing pores [26]. These results suggest that increasing pyrolysis temperature favored pore development within an appropriate range, whereas excessive heating could compromise the resulting pore structure. The effects of gas flow rate and heating rate varied with pyrolysis temperature, indicating that pore development depended on the combination of preparation conditions. Appropriate conditions can facilitate volatile removal and limit secondary reactions that reduce pore accessibility [27]. As shown in Fig. 2a and c, the BET specific surface area exhibited a quadratic response to gas flow rate. It increased as the flow rate rose from 200 to 325 mL min^{-1}, reached a high level near 425 mL min^{-1}, and declined with further increases. The initial increase may reflect more effective removal of volatile products and reduced secondary tar deposition within the pores. The subsequent decline suggests that excessive gas flow did not favor further surface area development, possibly because changes in heat transfer and volatile residence time altered the balance between carbonization and pore formation. Heating rate also exhibited a nonlinear effect, with its influence depending on pyrolysis temperature and gas flow rate (Fig. 2b and c). The BET specific surface area increased as the heating rate rose from 5 to approximately 6°C min^{-1}, remained high over 6–7°C min^{-1}, and decreased at higher rates. A moderate heating rate may balance heat transfer, volatile evolution, and carbon framework restructuring, thereby promoting pore development. Faster heating may disrupt this balance through abrupt devolatilization and local pressure buildup, potentially compromising pore wall integrity. Coordinated adjustment of the three preparation parameters is therefore necessary to promote pore formation while preserving the developed structure [28]. Collectively, the quadratic responses and interaction patterns indicate that surface area development was governed by the combined pyrolysis conditions

Preparation conditions were subsequently optimized using response surface methodology and a desirability function, with maximization of the BET specific surface area as the objective. The model identified an optimal pyrolysis temperature of 720.50°C, gas flow rate of 376.42 mL min^{-1}, and heating rate of 6.75°C min^{-1}, with a desirability value of 1.0. Under these conditions, the predicted BET specific surface area was 140.63 $m^2 g^{-1}$. The validation experiment yielded 141.93 $m^2 g^{-1}$, corresponding to a relative error of 0.92%. This close agreement supports the predictive performance of the model near the identified optimum and its application to selecting preparation conditions within the investigated range.

3.2 Directional evolution of micro-pores and surface chemical properties under thermal activation

Response surface analysis identified the optimal pyrolysis conditions within the experimental range, while characterization of the optimized sample further elucidated the structural basis established by this preparation process. The CO_2 adsorption performance of Bio@JQ, prepared by pyrolysis without further modification, is primarily governed by its carbon framework morphology, pore structure, and surface chemical environment. Accordingly, SEM-EDS, N_2 adsorption–desorption analysis, and spectroscopic characterization were combined to systematically examine its morphology, elemental composition, and pore structure across multiple scales. Morphological and pore structure analyses revealed the carbon framework formed during pyrolysis and the space accessible to gas molecules. Elemental mapping provided compositional evidence for further understanding nitrogen- and oxygen-containing surface structures.

As shown in Fig. 3a–e, Bio@JQ exhibited a characteristic irregular, honeycomb-like porous morphology, with surface openings of varying sizes and shapes. Interconnected pore walls formed a loose, three-dimensional carbon framework. Thin pore walls were observed in some regions, together with wrinkles, depressions, and fragmented edges, resulting in pronounced surface roughness and heterogeneity. Low-magnification images showed porous structures throughout different regions of the particles, while high-magnification images revealed details of the pore edges and walls. These observations indicated that the porous framework was relatively uniformly distributed throughout Bio@JQ. This morphology is consistent with pore formation through volatile release and progressive restructuring of the solid carbon framework during biomass pyrolysis. The exposed surface openings can serve as channels for gas transport into the carbon framework. They also demonstrate that jiuqu waste can be converted into carbon materials with an open pore structure through simple pyrolysis. EDS elemental mapping further revealed the elemental composition and spatial distribution of Bio@JQ (Fig. 3f–h). The C signal extended across the entire analyzed region, indicating that the pyrolysis product consisted primarily of a carbonaceous framework. Meanwhile, N and O signals were uniformly dispersed throughout the carbon matrix, with no pronounced large-scale elemental enrichment at the observed scale. These results indicate that carbonization produced a stable carbon framework while retaining a proportion of nitrogen- and oxygen-containing functional structures. The coexistence of C, N, and O highlights the multielement composition of Bio@JQ and provides a structural basis for subsequent analysis of its surface chemistry and CO_2 adsorption behavior.

SEM revealed the morphology of visible surface openings, whereas N_2 adsorption–desorption measurements provided additional information on the microscopic pore structure and gas-accessible space. As shown in Fig. 3i, Bio@JQ exhibited a sharp increase in uptake at low relative pressures, followed by a gradual approach to a plateau, yielding a characteristic type I adsorption isotherm. This rapid uptake at low pressures indicates abundant micropores that can undergo filling at low relative pressures, with micropore filling accounting for the major contribution to N_2 adsorption capacity. As relative pressure increased further, the increase in uptake became substantially smaller, indicating that the primary adsorption sites were approaching saturation. The adsorption and desorption branches nearly overlapped, with no pronounced broad hysteresis loop, further supporting predominantly

microporous adsorption behavior. Pore structure analysis yielded a specific surface area of 141.93 m^2 g^{-1} and a total pore volume of 0.0568 cm^3 g^{-1} for Bio@JQ. These values demonstrate that pyrolysis alone can produce a carbon material with measurable gas-accessible surface area and pore volume. Together with the isotherm characteristics, these results indicate that Bio@JQ contains both the open surface pores observed by SEM and micropore spaces that participate in gas adsorption at low pressures. The two characterization methods provide complementary evidence from morphological observations and adsorption responses, demonstrating the coexistence of pores at multiple scales. Larger openings help establish an open carbon framework and gas transport pathways, while micropores provide the principal adsorption space. Meanwhile, dispersed nitrogen- and oxygen-containing components further enrich the surface chemical environment.

Thus, the one-step preparation process produced a carbonaceous Bio@JQ framework with a multiscale pore structure and multielement composition. Its gas-accessible micropores and nitrogen- and oxygen-containing surface components jointly establish the material's structural basis and provide potential sites for CO_2 adsorption [29].

The carbon framework and surface chemical characteristics of Bio@JQ are shown in Fig. 4. The XRD pattern exhibited broad diffraction features associated with the (002) and (100) planes at 2θ values of 23–25° and 43°, respectively. These features indicate limited order in carbon layer stacking and in-plane arrangement, consistent with a low degree of graphitization (Fig. 4a). The broad (002) feature reflects irregular carbon layer stacking, whereas the weaker (100) feature is associated with local in-plane order [30, 31]. Together, these observations indicate that the carbon framework of Bio@JQ is predominantly disordered, while retaining some turbostratic carbon domains with short-range order. Thus, pyrolysis of jiuqu waste produced a carbon material characterized primarily by low structural order, rather than a graphitic structure with pronounced long-range order.

FTIR spectroscopy further revealed the diverse chemical structures and local chemical environments retained on the Bio@JQ surface (Fig. 4b). Peak deconvolution within the 1000–1800 cm^{-1} region identified the most prominent absorption peak at 1430 cm^{-1} (Fig. 4d). This vibrational response may be associated with carboxylate structures, with possible overlapping contributions from aliphatic C–H bending vibrations and carbonate species. The strong absorption therefore reflects the combined contributions of multiple vibrational modes. In contrast, the weak absorption near 1000–1100 cm^{-1} is associated with C–O vibrations and may also include contributions from inorganic oxygen-containing components [32]. These results indicate that Bio@JQ prepared through the one-step process retains oxygen-containing structures in different chemical environments, in addition to highly condensed carbon structures. Within the 2800–3000 cm^{-1} region, the absorption peaks at 2920 and 2850 cm^{-1} can be assigned to asymmetric and symmetric methylene ($–CH_2–$) stretching vibrations, respectively, accompanied by weaker methyl-related absorptions (Fig. 4e). These features indicate the retention of some aliphatic segments and incompletely aromatized structures in Bio@JQ. Together with the XRD results, they suggest that pyrolysis promoted carbon restructuring and local ordering while leaving some

nonaromatic components, reflecting the chemical heterogeneity of biomass-derived carbon. A broad absorption band was also observed at 3400–3500 cm^{-1}, primarily arising from O–H stretching vibrations of hydroxyl groups and adsorbed water molecules (Fig. 4f). This broad band reflects overlapping hydroxyl vibrations in different local chemical environments, with hydrogen bonding potentially contributing to band broadening.

The XPS survey spectrum showed distinct C 1s, O 1s, and N 1s signals, consistent with the EDS results and further confirming the presence of carbon, oxygen, and nitrogen on the Bio@JQ surface (Fig. 4c). The high-resolution C 1s spectrum was dominated by a peak at 284–285 eV, assigned to C–C/C = C structures (Fig. 4g). This dominant peak indicates that the carbon framework constitutes the principal surface carbon component, consistent with the low structural order revealed by XRD. Additional peaks at higher binding energies indicate that some carbon atoms occupy local chemical environments distinct from those of the main carbon framework. These features reveal diverse carbon bonding configurations across the surface. The O 1s spectrum exhibited a major peak near 532 eV, which can be attributed to overlapping contributions from carbonyl oxygen, ether oxygen, and other oxygen-containing structures [33]. A weaker feature on the higher-binding-energy side further indicates the presence of distinct oxygen chemical environments (Fig. 4h). These results corroborate the O–H- and C–O-related absorptions observed by FTIR, supporting the presence of multiple oxygen-containing functional structures on the Bio@JQ surface. The N 1s spectrum showed characteristic components near 398 and 400 eV, tentatively assigned to pyridinic and pyrrolic nitrogen, respectively, with the peak near 400 eV exhibiting greater intensity (Fig. 4i). These results indicate that some nitrogen atoms are incorporated into the carbon framework as nitrogen-containing heterocycles, creating local electronic environments distinct from those of pure carbon structures.

Collectively, the XRD, FTIR, and XPS results indicate that Bio@JQ contains a carbon framework with low structural order and local turbostratic domains. It also retains aliphatic structures, oxygen-containing functional groups, and nitrogen-containing components, resulting in a complex surface with multiple bonding states and chemical environments. These characteristics identify the pyrolysis product of jiuqu waste as a biomass-derived carbon material featuring structural defects, disordered regions across multiple scales, and diverse surface chemical environments, rather than a simple graphitized carbon.

3.3 Evaluation of CO_2 adsorption separation efficiency, thermodynamics and stability

Bio@JQ prepared solely by pyrolysis exhibited appreciable CO_2 adsorption capacity, with its equilibrium adsorption performance influenced by both pressure and temperature. As shown in Fig. 5a, Bio@JQ adsorbed CO_2 throughout the tested temperature range of 273.15–318.15 K, and uptake increased with equilibrium pressure. The isotherms rose steeply at low pressures, indicating effective adsorption at low CO_2 partial pressures. As pressure increased further, the slopes gradually decreased, consistent with progressive micropore filling and occupation of high-affinity adsorption sites. None of the isotherms

reached a clear plateau near 1 bar, indicating that CO_2 uptake continued to increase throughout the tested pressure range. At 1 bar, the CO_2 adsorption capacities of Bio@JQ were approximately 2.32, 1.76, and 1.36 mmol g^{-1} at 273.15, 303.15, and 318.15 K, respectively. The higher capacity at lower temperatures reflects the favorable effects of decreasing temperature on molecular adsorption and pore filling [34]. Meanwhile, an uptake of approximately 1.76 mmol g^{-1} at 303.15 K demonstrates that the material retained CO_2 capture capability near room temperature. Adsorption capacity decreased progressively with increasing temperature, consistent with the thermodynamic characteristics of an exothermic adsorption process. This trend further confirms the pronounced temperature dependence of CO_2 adsorption on Bio@JQ.

Figure 5b compares Bio@JQ with previously reported biochars in terms of preparation temperature, specific surface area, and CO_2 adsorption capacity, illustrating performance differences among preparation strategies. Compared with many carbon materials requiring multistep activation or chemical modification, Bio@JQ offers favorable CO_2 adsorption performance through a one-step process using jiuqu waste as the feedstock (Table S1). This preparation route avoids additional activation steps while valorizing waste biomass and imparting gas adsorption functionality [35]. At 1 bar, Bio@JQ achieved CO_2 uptakes of 2.32 and 1.76 mmol g^{-1} at 273.15 and 303.15 K, respectively. These results demonstrate that a one-step process can convert jiuqu waste into carbon structures with adsorption activity, highlighting its potential as a precursor for functional carbon materials.

The isosteric heat of adsorption (Q_{st}) further elucidated the energetic interactions between Bio@JQ and CO_2 molecules (Fig. 5c). Within the uptake range jointly covered by the isotherms at different temperatures, Qst was approximately 19–21 kJ mol^{-1} at low loading. It gradually increased with uptake, reaching 27–28 kJ mol^{-1} at approximately 1.0 mmol g^{-1}. This range is generally associated with predominantly physical CO_2 adsorption and is consistent with the decrease in adsorption capacity at higher temperatures [29]. Variations in Q_{st} at low loading are associated with preferential occupation of adsorption sites with different affinities. As uptake increases, interactions among CO_2 molecules within the pores and the progressive formation of an adsorbed layer further strengthen the energetic response. Thus, the loading-dependent Q_{st} provides complementary energetic evidence that pore filling and surface interactions both contribute to CO_2 adsorption on Bio@JQ.

In addition to its adsorption capacity, Bio@JQ exhibited good cycling stability (Fig. 5d). After 5, 15, 30, and 45 adsorption–regeneration cycles, it retained 99.13%, 96.55%, 94.04%, and 91.88% of its initial CO_2 adsorption capacity, respectively. The material retained more than 90% of its initial capacity after 30 cycles, and its uptake remained approximately 2.12 mmol g^{-1} even after 45 cycles. These results indicate that Bio@JQ largely maintained its adsorption performance during repeated regeneration. Capacity changes at the different cycling intervals showed a relatively slow, continuous decline without pronounced rapid deterioration, demonstrating good cycling durability under the tested conditions. For a biomass-derived carbon material prepared without further activation, the substantial capacity retention

after 45 cycles is encouraging. It indicates that Bio@JQ combines favorable adsorption capacity with potential for use in regenerable CO_2 capture processes.

Overall, direct pyrolysis produced a Bio@JQ carbon framework with a multiscale pore structure and nitrogen- and oxygen-containing surface functionalities. The material achieved a CO_2 adsorption capacity of approximately 2.32 mmol g^{-1} at 273.15 K and 1 bar and retained 91.88% of its initial capacity after 45 adsorption–regeneration cycles. Its simplified preparation, consistent equilibrium adsorption performance, and good cycling retention collectively demonstrate the feasibility of producing CO_2 adsorbents through direct pyrolysis of jiuqu waste. This approach offers a potential pathway for converting waste biomass into functional carbon materials.

3.4 Further discussion

The CO_2 adsorption performance of biomass-derived carbons depends on the combined effects of pore accessibility, pore size distribution, and surface chemistry. These properties should be considered in relation to the intended adsorption conditions rather than optimized independently. Sevilla and Fuertes demonstrated that carbons prepared under mild activation conditions could exhibit favorable CO_2 uptake despite having lower surface areas than more extensively activated samples [36]. Their results emphasized the importance of narrow micropores for low-pressure adsorption. Accordingly, developing biochar adsorbents requires coordinated control of accessible adsorption space and molecular affinity, rather than simply maximizing BET specific surface area.

In this study, direct pyrolysis converted jiuqu waste into a porous carbon framework while retaining nitrogen- and oxygen-containing surface structures. The response surface results indicate that pore development depends on interactions among pyrolysis temperature, heating rate, and N_2 flow rate. These interactions suggest that thermal processing should balance component decomposition, volatile removal, and carbon framework restructuring. The resulting honeycomb-like morphology provides an open framework, while the type I N_2 adsorption isotherm supports the presence of accessible micropores. Together, these observations establish a structural basis for CO_2 adsorption without additional chemical modification. Nevertheless, because BET specific surface area was the optimization response, the identified conditions represent the optimum for this textural parameter within the experimental range. Direct optimization of CO_2 uptake could further clarify whether the same conditions maximize adsorption performance.

A notable feature of Bio@JQ is its CO_2 uptake of 2.32 mmol g^{-1} at 273.15 K and 1 bar despite a BET specific surface area of 141.93 m^2 g^{-1}. This combination suggests that total surface area alone does not adequately describe its adsorption behavior. Research on steam-assisted pyrolysis biochars has shown that N_2 adsorption at 77 K can underestimate narrow microporosity because of diffusion restrictions. Consequently, the surface area measured using N_2 should not be assumed to represent all spaces accessible to CO_2 at higher temperatures [37]. For Bio@JQ, this provides a plausible explanation

for the coexistence of moderate BET surface area and appreciable CO_2 uptake, although additional pore analysis is required to establish the contribution of narrow micropores.

Based on its structural and adsorption characteristics, CO_2 capture by Bio@JQ can be interpreted as a process involving micropore filling and noncovalent interactions with pore walls (Fig. 6). The porous carbon framework provides gas transport pathways, while gas-accessible micropores offer confinement and space for CO_2 accumulation. Dispersion interactions between CO_2 molecules and carbon walls help stabilize adsorption. When pore dimensions approach the molecular scale, overlapping adsorption potentials from opposing walls may further strengthen local adsorption [38]. Meanwhile, nitrogen- and oxygen-containing structures may modify local electronic distributions and surface polarity, enhancing electrostatic and induction interactions associated with the CO_2 quadrupole moment and thereby modulating local adsorption affinity. Together, confinement and surface interactions promote CO_2 adsorption and pore filling, while molecular desorption during regeneration restores the available adsorption space.

The thermodynamic and cycling results complement this structural interpretation. The decrease in uptake with increasing temperature and the Q_{st} range of approximately 19–28 kJ mol^{-1} are consistent with predominantly physical adsorption. The increase in Q_{st} with loading may involve interactions among confined CO_2 molecules, although this trend alone cannot distinguish adsorbate interactions from changes in the sampled adsorption environments [39]. Retention of 91.88% of the initial capacity after 45 adsorption–regeneration cycles further demonstrates sustained reversibility under the tested conditions. These results support an adsorption mechanism involving recoverable pore occupation and noncovalent interactions. They do not, however, directly establish structural preservation during cycling, which could be examined through characterization of regenerated samples.

Comparison with reported adsorbents should consider preparation requirements alongside adsorption capacity. Bio@JQ achieved an uptake of 1.76 mmol g^{-1} at 303.15 K and 1 bar through direct pyrolysis, offering a combination of near-ambient adsorption capability and a simplified preparation route. Its practical significance lies in obtaining adsorption functionality from jiuqu waste without added activating or doping agents. Comparisons across studies should nevertheless account for differences in temperature, pressure, feedstock, and regeneration conditions [40]. The present results establish the feasibility of this preparation strategy, while matched-condition comparisons would better assess its performance relative to other waste-derived carbons.

From a resource utilization perspective, the approach links solid fermentation waste valorization with the production of reusable CO_2 adsorbents. Eliminating additional chemical activation simplifies processing and avoids chemical consumption associated with that step. However, overall economic and environmental performance also depends on feedstock drying, pyrolysis energy demand, N_2 consumption, biochar yield, and regeneration requirements. Future optimization could therefore combine CO_2 uptake and cycling retention with material yield and energy use as process objectives. Mixed-gas

adsorption, humid breakthrough experiments, and working-capacity measurements would further connect the equilibrium results to practical separation conditions [21]. Collectively, this study provides a basis for developing jiuqu-derived adsorbents through coordinated control of thermal processing, accessible microporosity, and retained surface chemistry.

4. Conclusions

In this study, Bio@JQ was prepared from jiuqu waste by optimizing pyrolysis conditions using response surface methodology, without additional chemical modification or activation. Structural characterization, adsorption isotherms, isosteric heats of adsorption, and cycling tests were combined to investigate its structure–adsorption relationships. The main conclusions are as follows:

(1) Bio@JQ prepared under the optimized conditions exhibited a honeycomb-like porous morphology and gas-accessible micropores, with a specific surface area of 141.93 $m^2 g^{-1}$ and a total pore volume of 0.0568 $cm^3 g^{-1}$. Its carbon framework had low overall structural order while retaining local turbostratic domains and nitrogen- and oxygen-containing chemical environments. These results demonstrate that direct pyrolysis can simultaneously develop pore space and preserve diverse surface chemical structures.

(2) CO_2 uptake increased with pressure and decreased with temperature, consistent with exothermic adsorption. At 1 bar, the equilibrium adsorption capacities were approximately 2.32, 1.76, and 1.36 mmol g^{-1} at 273.15, 303.15, and 318.15 K, respectively. These results demonstrate a capacity advantage at low temperatures and CO_2 adsorption capability near ambient temperature.

(3) Structural characterization and adsorption results jointly support a mechanism involving micropore filling and noncovalent interactions with pore walls. Nitrogen- and oxygen-containing structures may influence adsorption affinity by modifying local electronic distributions and polarity. The isosteric heats of adsorption within the valid calculation range are consistent with an important contribution from physical interactions, indicating that pore space and surface chemistry jointly influence adsorption behavior.

(4) Bio@JQ exhibited good reusability, retaining 94.04% and 91.88% of its initial capacity after 30 and 45 adsorption–regeneration cycles, respectively. Its adsorption capacity remained approximately 2.04 mmol g^{-1} in the 45th cycle. These findings demonstrate that pyrolysis alone can convert jiuqu waste into carbon materials combining CO_2 adsorption capacity with cycling durability, providing a feasible route for converting solid fermentation waste into functional materials.

Declarations

Declaration of competing interest

The authors declare that they have no known competing financial interests or personal relationships that could have appeared to influence the work reported in this paper.

CRediT authorship contribution statement

Dexin Xu: Writing– original draft,Writing– review & editing, Visualization and Software. **Xuyao Qi:** Writing– review & editing, Funding acquisition and Project administration. **Mujun Chen:** Methodology, Conceptualization and Software. **Chunxi Wu:** Data curation and Investigation. **Lanjun Zhang:** Resources and Methodology. **Fusheng Wang:** Data curation and Formal analysis. **Leilin Zhang:** Methodology and Data curation. **Yaqi Qin:** Resources and Formal analysis.

Acknowledgements

The authors deeply appreciate the financial support provided by the Natural Science Foundation of Jiangsu Province (No. BK20240104), the Science & Technology Fundamental Resources Investigation Program (No. 2025FY101700), the National Natural Science Foundation of China (No. 52574297).

Declaration of generative AI use

During the preparation of this manuscript, the authors employed Chat GPT (Open AI) exclusively for English language polishing and editing. The authors have thoroughly reviewed all AI-assisted outputs and take full responsibility for every part of this publication.

References

1. Chen WQ, Foo JCL, Veksha A, Chan W-P, Ge LY, Lisak G. Unveiling key impact parameters and mechanistic insights towards activated biochar performance for carbon dioxide reduction. Bioresour Technol 2024;411:131355 https://doi.org/10.1016/j.biortech.2024.131355.
2. Etzi M, Sartoretti E, Bensaid S, Allione M, Ferraris S, Castellino M, Armandi M. Tuning microporosity and surface chemistry: The synergistic effect of KOH and urea on CO_2 capture performance of sucrose-derived activated carbons. Chem Eng J (Lausanne) 2025;521:167166 https://doi.org/10.1016/j.cej.2025.167166.
3. Martín-Lara M, Muñoz-Batista MJ, Blázquez G, Pereira L, Quintana A, Calero M. Turning plastic and biomass waste into adsorbents: CO_2/CH_4 separation and comparison with commercial carbons. Waste Manag 2026;210:115223 https://10.1016/j.wasman.2025.115223.
4. Sun Y, Jia J, Liu Z, Liu Z, Huo L, Zhao L, et al. Heteroatom-doped biochar devised from cellulose for CO_2 adsorption: a new vision on competitive behavior and interactions of N and S. Biochar 2023;5(1):76 https://10.1007/s42773-023-00275-1.
5. Zhang P, Li C, Huo L, Zhao L, Yao Z. Synergistic enhancement of CO_2 adsorption on MgO-nanoparticle-loaded corn straw biochar: insights from ball milling pathways and DFT calculations.

Separation and Purification Technology 2026;409:139272 https://doi.org/10.1016/j.seppur.2026.139272.

6. Cao W, Xu H, Zhang X, Xiang W, Qi G, Wan L, Gao B. Novel post-treatment of ultrasound assisting with acid washing enhance lignin-based biochar for CO_2 capture: Adsorption performance and mechanism. Chem Eng J (Lausanne) 2023;471:144523 https://doi.org/10.1016/j.cej.2023.144523.
7. Zhang P, Luo J, Huo L, Zhao L, Yao Z. Straw-derived porous biochars by ball milling for CO_2 capture: Adsorption performance and enhanced mechanisms. Industrial Crops and Products 2025;229:121000 https://doi.org/10.1016/j.indcrop.2025.121000.
8. Gargiulo V, Gomis-Berenguer A, Giudicianni P, Ania CO, Ragucci R, Alfè M. Assessing the Potential of Biochars Prepared by Steam-Assisted Slow Pyrolysis for CO_2 Adsorption and Separation. Energy & Fuels 2018;32(10):10218-27 https://10.1021/acs.energyfuels.8b01058.
9. Zhang C, Ji Y, Li C, Zhang Y, Sun S, Xu Y, et al. The Application of Biochar for CO_2 Capture: Influence of Biochar Preparation and CO_2 Capture Reactors. Ind Eng Chem Res 2023;62(42):17168-81 https://10.1021/acs.iecr.3c00445.
10. Luo J, Chen Y, Zhang X, Ma R, Huang H, Sun S, et al. Microwave-induced preparation of MgO-loaded N-rich porous biochar from marine biomass for efficient CO_2 capture and mechanism exploration via theoretical calculation. Journal of Cleaner Production 2023;405:136915 https://doi.org/10.1016/j.jclepro.2023.136915.
11. Arjona-Jaime P, Morales-Ospino R, Izquierdo MT, Chazaro-Ruiz LF, Celzard A, Rangel-Mendez R, Fierro V. Ca-modified biochar by microwave irradiation for robust CO_2 capture under realistic flue gas conditions. Chem Eng J (Lausanne) 2025;525:170349 https://doi.org/10.1016/j.cej.2025.170349.
12. Jonnalagadda M, Ibrahim SM, Shair OHM, Mutyala S. Porous carbon supported calcium oxide for CO_2 adsorption and separation of CO_2/CH_4. Environ Technol 2022;43(3):460-8 https://10.1080/09593330.2020.1791973.
13. Ahmed S, Hossain D, Dipti SS, Karim MA, Azad MAK. Metals incorporated agricultural waste corn Cob-based biochar used as an adsorbent for CO_2 capturing. Scientific Reports 2025;16(1):1470 https://10.1038/s41598-025-31699-3.
14. Li D, Sun L, He R, Xiao G, Zhu D, Wang W, Ye J. Hierarchically porous MgO/biochar composites for efficient CO_2 capture: Structure, performance and mechanism. Chem Eng J (Lausanne) 2024;498:155607 https://doi.org/10.1016/j.cej.2024.155607.
15. Zhang M, Liang C, Duan L, Chen H. Fe-Ce modified biochar reinforced CaO-Char system enables efficient simultaneous SO_2/CO_2 removal: By enhancing synergistic SO_2 reduction in the carbonation step. Chem Eng J (Lausanne) 2025;525:170851 https://doi.org/10.1016/j.cej.2025.170851.
16. Yameen MZ, Naqvi SR, Juchelková D, Khan MNA. Harnessing the power of functionalized biochar: progress, challenges, and future perspectives in energy, water treatment, and environmental sustainability. Biochar 2024;6(1):25 https://10.1007/s42773-024-00316-3.

17. Quan C, Zhou Y, Wang J, Wu C, Gao N. Biomass-based carbon materials for CO_2 capture: A review. Journal of CO_2 Utilization 2023;68:102373 https://doi.org/10.1016/j.jcou.2022.102373.
18. Petri E, Heigl E-M, Fasolini A, Zeilerbauer L, Giovannucci M, Küçükağa Y, et al. Conversion of biodigestate into activated carbon for electrochemical application: Process performance and life cycle assessment. Carbon 2024;226:119221 https://doi.org/10.1016/j.carbon.2024.119221.
19. Kumar A, Singh E, Mishra R, Lo S-L, Kumar S. A green approach towards sorption of CO_2 on waste derived biochar. Environ Res 2022;214:113954 https://doi.org/10.1016/j.envres.2022.113954.
20. Xu Y, Zhang B, Ni D, Yang Y, Yang F, Kong X, Tu H. The multi-scale structures and physicochemical properties changes of wheat starch during high-temperature Daqu preparation process. Food Chem X 2025;29:102824 https://10.1016/j.fochx.2025.102824.
21. Kane S, Miller SA. Predicting biochar properties and pyrolysis life-cycle inventories with compositional modeling. Bioresour Technol 2024;399:130551 https://doi.org/10.1016/j.biortech.2024.130551.
22. Correia I, Ilkaeva M, Castellino M, Bocchini S, Novais RM, Mafra L, et al. Impact of pyrolysis heating methods on biochars with enhanced CO_2/N_2 separation and their incorporation in 3D-printed composites. Journal of Environmental Chemical Engineering 2024;12(5):113875 https://doi.org/10.1016/j.jece.2024.113875.
23. Umar M, Yusuf BO, Aliyu M, Hussain I, Alhassan AM, Awad MM, et al. Advancing frontiers in CO_2 capture: The renaissance of biomass-derived carbon materials. Coord Chem Rev 2025;526:216380 https://doi.org/10.1016/j.ccr.2024.216380.
24. Huang Y-Y. The temperature dependence of isosteric heat of adsorption on the heterogeneous surface. J Catal 1972;25(1):131-8 https://doi.org/10.1016/0021-9517(72)90210-2.
25. Karandagaspitiya CO, Matuszek K, Webley PA, Guo Y. Incorporation of azolate-based ionic liquids into MCM-41 silica for direct air capture of CO_2. Chem Eng J (Lausanne) 2026;534:174849 https://doi.org/10.1016/j.cej.2026.174849.
26. Salinas-Farran L, Mosonik MCA, Jervis R, Marathe S, Rau C, Volpe R. Tracked evolution of single biochar particle's morphology during pyrolysis in operando x-ray micro-computed tomography. Biochar 2024;6(1):86 https://10.1007/s42773-024-00374-7.
27. Paudel PP, Park S, Kim SJ, Kim SY, Kang KS, Kim KJ, Kim DH. Comprehensive study on microwave pyrolysis process variables and operating modes for optimized biochar production. Bioresour Technol 2025;437:133120 https://10.1016/j.biortech.2025.133120.
28. Ma R, Luo J, Duan X, Sheng Y, Wang S, Zhang D, et al. Novel laser-driven fast pyrolysis of biomass: Insights into biochar characteristics and applications. Bioresour Technol 2025;436:132986 https://10.1016/j.biortech.2025.132986.
29. Guo P, Xue R, Zou Q, Ma X, Su C, Zeng Z, Li L. Enhanced Ultramicropore of Biomass-Derived Porous Carbon for Efficient and Low-Energy CO_2 Capture: Integration of Adsorption and Solar Desorption. Energy & Environmental Materials 2026;9(2):e70140 https://doi.org/10.1002/eem2.70140.

30. Bagheri A, Taghavi S, Bellani S, Salimi P, Beydaghi H, Panda JK, et al. Venice's macroalgae-derived active material for aqueous, organic, and solid-state supercapacitors. Chem Eng J (Lausanne) 2024;496:153529 https://doi.org/10.1016/j.cej.2024.153529.
31. Cui J, Rao Y, Gao J, Zhang H, Lin C, Zhao J, et al. Data-driven intelligent carbonization unifies diverse biomass into high-performance hard carbon negative electrodes. Nat Commun 2026;17(1):3885 https://10.1038/s41467-026-70411-5.
32. Iswardi AH, Hubble AH, Lehmann J, Goldfarb JL. Can batch lab-scale studies of slow pyrolysis describe biochar yields and properties upon upscaling to a continuous auger kiln? Journal of Cleaner Production 2025;496:145150 https://doi.org/10.1016/j.jclepro.2025.145150.
33. Zhao Q, Cui J, Hou Y, Pei P. Effect of pyrolysis temperature on physicochemical characteristics and toxic elements for grub manure-derived biochar. RSC Advances 2024;14(38):27883-93 https://10.1039/d4ra03778b.
34. Xuan K, Wu J, Zhang Y, Zhong L, Othman RM, Lithoxoos GP, et al. Quantitative analysis of temperature-dependent transition of CO_2 adsorption mechanisms by adsorbents – From enthalpy-driven interactions to pore-filling capture. Chem Eng J (Lausanne) 2026;530:173381 https://doi.org/10.1016/j.cej.2026.173381.
35. Ghanbarpour Mamaghani Z, Hawboldt KA, MacQuarrie S, Katz MJ. Impact evaluation of coexisting gas CO on CO_2 adsorption on biochar derived from softwood shavings. Separation and Purification Technology 2024;338:126529 https://doi.org/10.1016/j.seppur.2024.126529.
36. Sevilla M, Fuertes AB. Sustainable porous carbons with a superior performance for CO2 capture. Energy & Environmental Science 2011;4(5):1765-71 https://10.1039/c0ee00784f.
37. Gargiulo V, Gomis-Berenguer A, Giudicianni P, Ania CO, Ragucci R, Alfè M. Assessing the Potential of Biochars Prepared by Steam-Assisted Slow Pyrolysis for CO(2) Adsorption and Separation. Energy Fuels 2018;32(10):10218-27 https://10.1021/acs.energyfuels.8b01058.
38. Wang X, Li X, Shi Y, Li Y, Sui Z, Wang J, Xu X. Decoupling pore structure from surface chemistry to elucidate structure-performance relationships in SF6 and CO_2 capture. Chem Eng J (Lausanne) 2026;529:173247 https://doi.org/10.1016/j.cej.2026.173247.
39. Zhang H, Jiang F, Zhang X, Hu S, Li J, Zhang H, Liu K. CO_2 adsorption performance of nitrogen-doped activated carbon from banana pseudo-stem by urea-assisted high-pressure CO_2-Hydrothermal treatment. Separation and Purification Technology 2025;366:132773 https://doi.org/10.1016/j.seppur.2025.132773.
40. Patel H, Mohanty A, Misra M. Post-combustion CO2 capture using biomass based activated porous carbon: Latest advances in synthesis protocol and economics. Renewable and Sustainable Energy Reviews 2024;199:114484 https://doi.org/10.1016/j.rser.2024.114484.

Figures

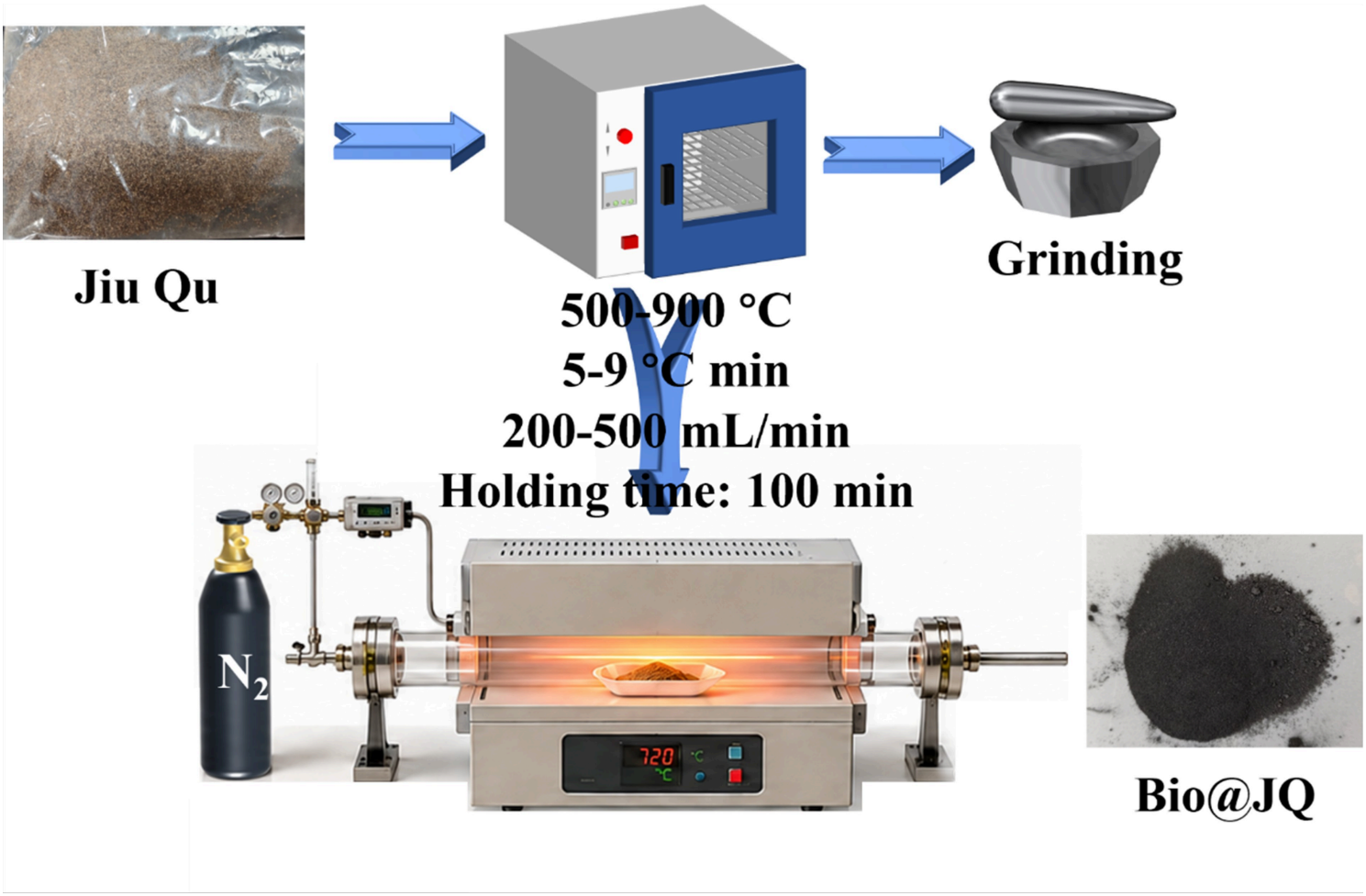

Figure 1

Preparation process for jiuqu-derived biochar

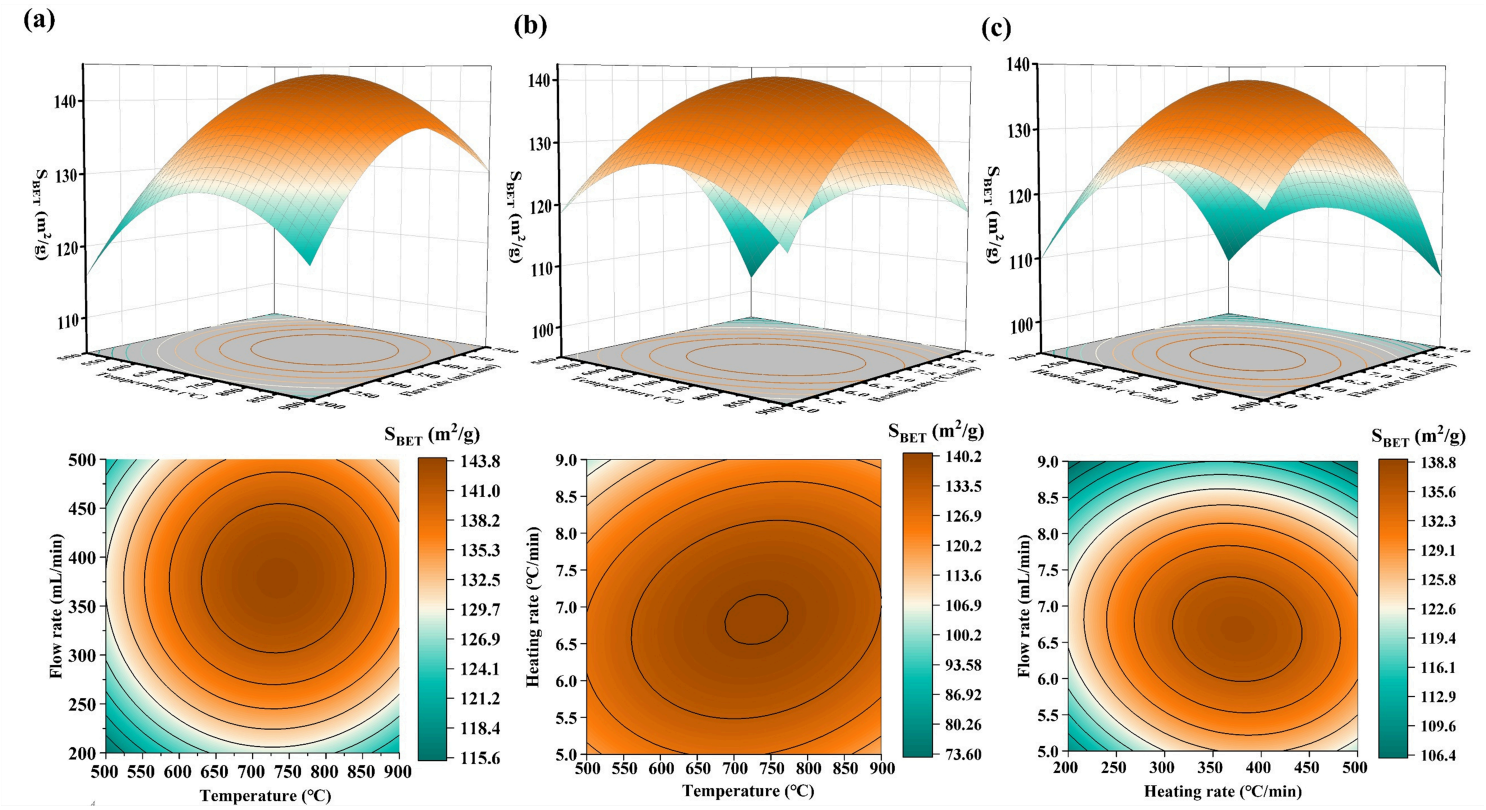

Figure 2

Response values of biochar specific surface area: (a) Temperature and flow rate; (b) Temperature and heating rate; (c) Flow rate and heating rate

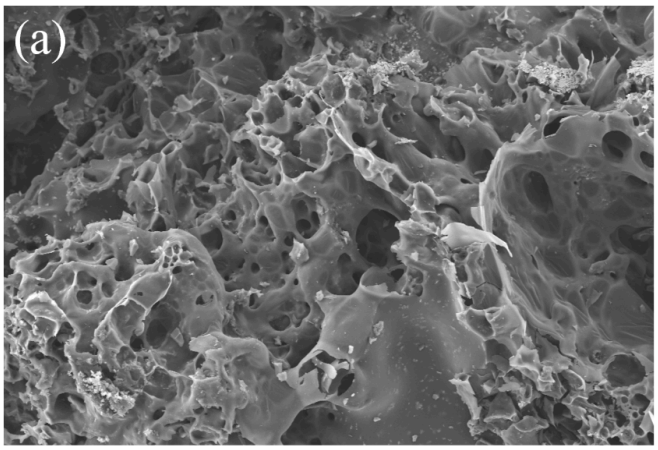

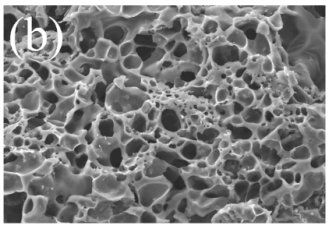

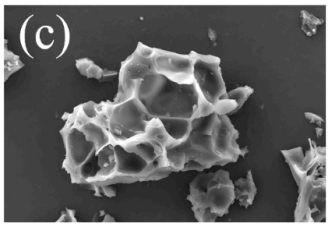

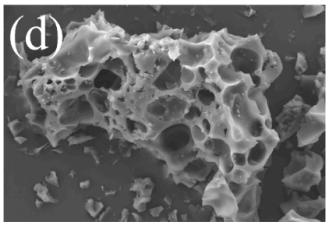

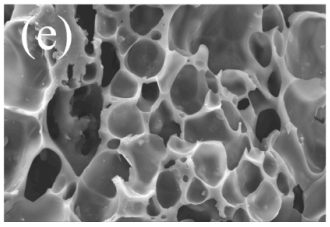

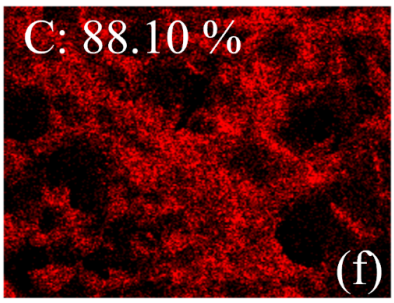

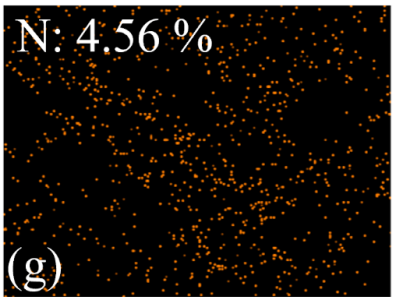

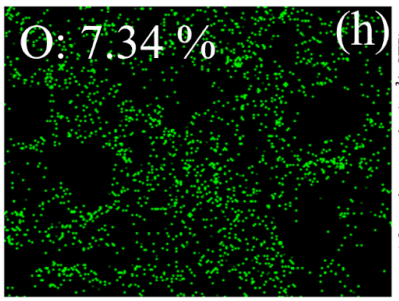

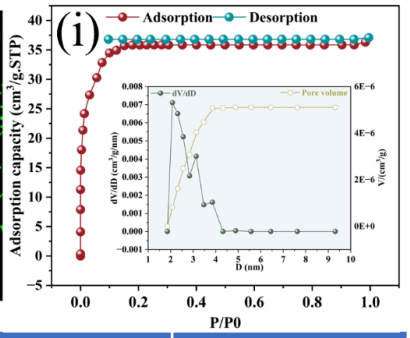

Specific surface area (m^2/g)	Total pore volume (nm)	Pore diameter (nm)
141.93	0.0568	1.6008

Figure 3

Morphology and pore structure of biochar: (a–e) SEM images at different magnifications; (f–h) EDS elemental maps of C, N, and O; (i) N_2 adsorption–desorption isotherms

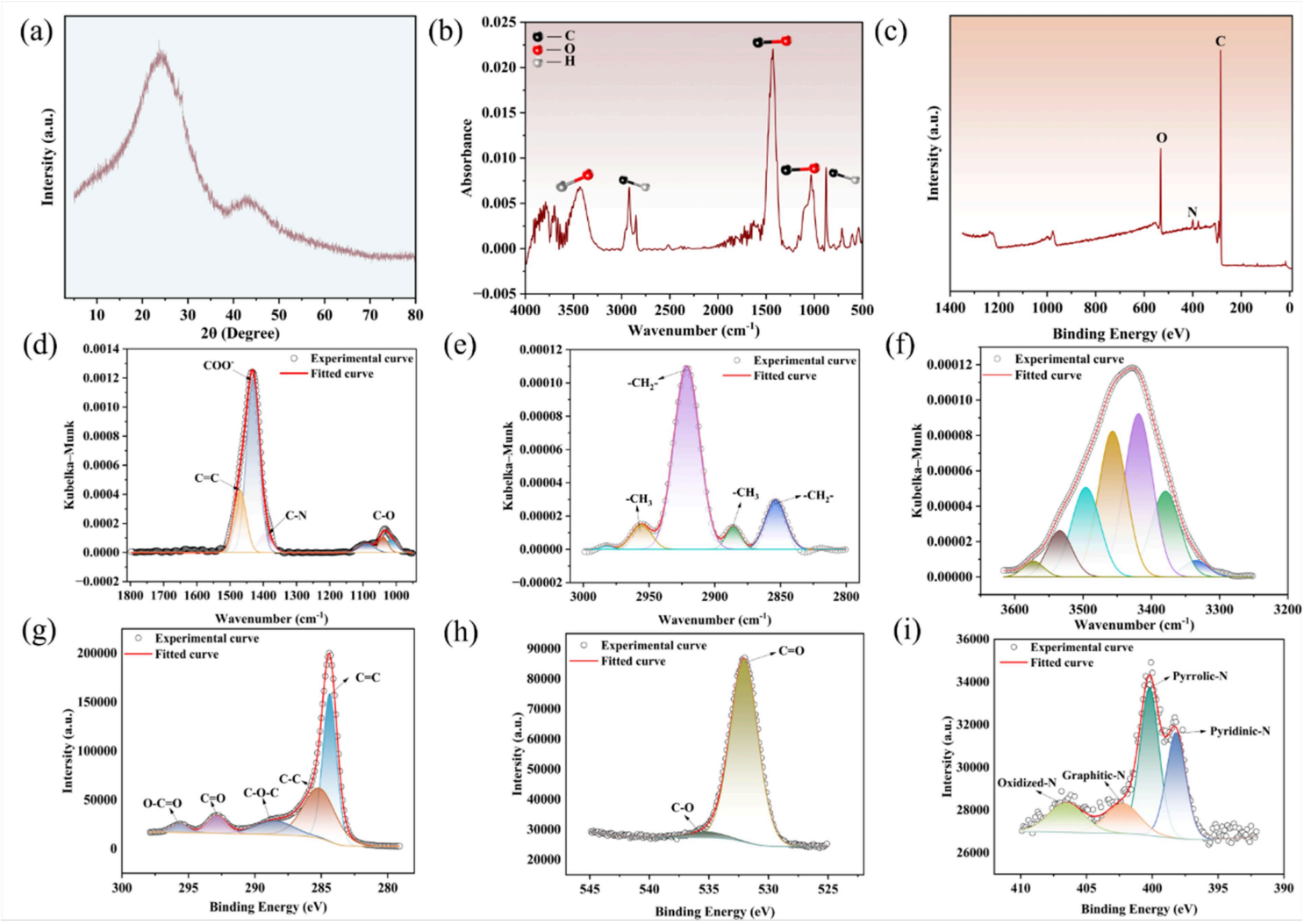

Figure 4

Carbon framework and surface chemical characteristics of biochar: (a) XRD pattern; (b) FTIR spectrum; (c) XPS survey spectrum; (d–f) deconvoluted FTIR spectra of carbon–oxygen groups, alkyl side chains, and hydroxyl groups, respectively; (g–i) high-resolution XPS spectra of C 1s, O 1s, and N 1s, respectively

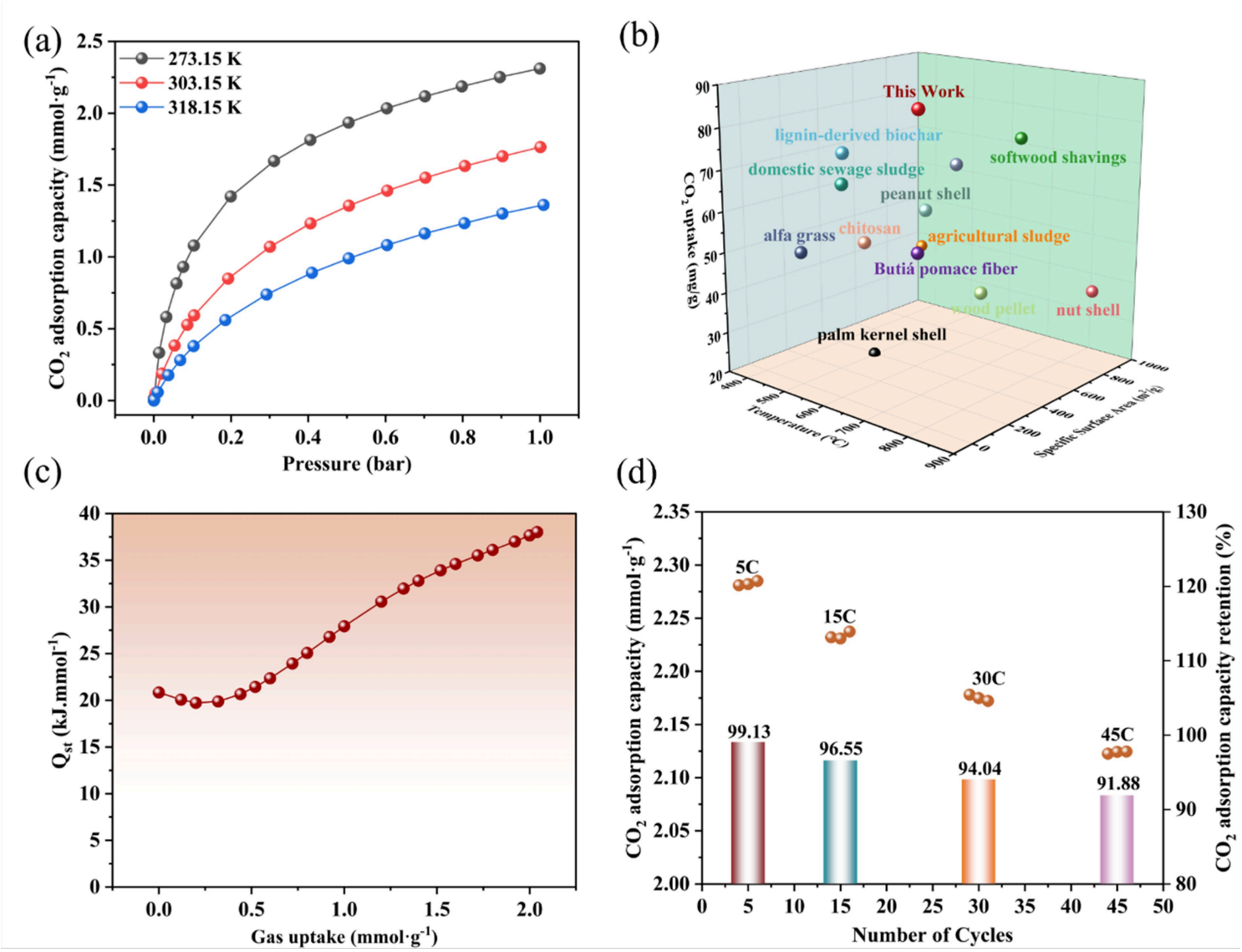

Figure 5

CO_2 adsorption performance of biochar: (a) CO_2 adsorption isotherms at different temperatures; (b) comparison of CO_2 adsorption capacities of waste-derived adsorbents; (c) isosteric heat of CO_2 adsorption; (d) adsorption–regeneration cycling performance

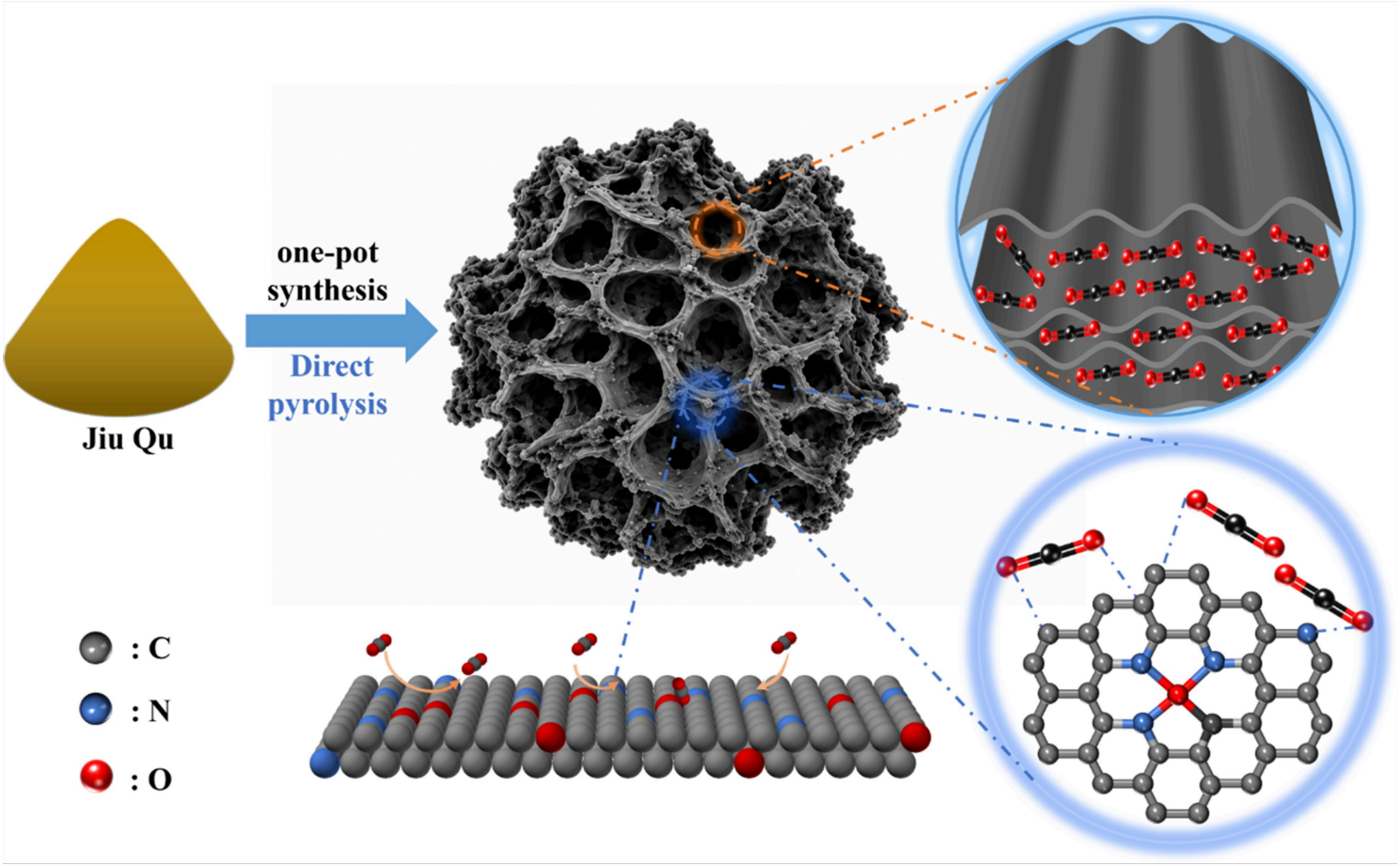

Figure 6

Proposed CO_2 capture mechanism of Bio@JQ

Supplementary Files

This is a list of supplementary files associated with this preprint. Click to download.

- Supplementaryinformation.docx